Cite this as:
Y. Chen, A. Erbe: *Surface Science*, **607**, 39-46 (**2013**).

Final copy-edited version of the manuscript is available from:
http://dx.doi.org/10.1016/j.susc.2012.08.006

In situ spectroscopic ellipsometry during electrochemical treatment of zinc in alkaline carbonate electrolyte

Ying Chen[a,b], Andreas Erbe[a,*]

[a] *Max-Planck-Institut für Eisenforschung GmbH, Department of Interface Chemistry and Surface Engineering, Max-Planck-Str. 1, 40237 Düsseldorf, Germany*
[b] *Center for Electrochemical Sciences, Ruhr-Universität Bochum, Universitätstr. 150, 44780 Bochum, Germany*

Abstract

In situ spectroscopic ellipsometry (SE, 297–820 nm, 4.4–1.5 eV) during electrochemical oxidation/reduction of zinc in alkaline carbonate electrolyte was performed using a specially designed optical-electrochemical cell. The growth and shrinkage of the interfacial layer on Zn was analysed on the basis of Lekner's first order perturbation theory. For non-absorbing thin films on metal surfaces, an algorithm has been derived to extract the thickness of a surface film directly from ellipsometric data without the need of optical modelling. During cyclic voltammetry (CV), a rapid decrease/increase in the layer thickness in the reduction/oxidation peak has been found. In the potential regime where the surface is oxide-covered, the layer thickness increases/decreases linearly with potential in anodic/cathodic scans. The density of the interfacial region in this regime is constant. During chronoam-

*Corresponding author; Phone: +49 211 6792 890, Fax: +49 211 6792 218
Email address: a.erbe@mpie.de, aerbe@arcor.de (Andreas Erbe)

[1] Abbreviations used: CA – chronoamperometry, CV – cyclic voltammetry, OCP – Open Circuit Potential, PCSA – Polariser-Compensator-Sample-Analyser, SE – spectroscopic ellipsometry, SHE – Standard Hydrogen Electrode

perometric experiments, a fast correlating jump in thickness was found after potential jumps. An ageing of the films is observed in the absorption spectrum (from the ellipsometric parameter Ψ), which shows changes until ≈30 min after potential jumps. Analysis of the current transients points to continuous dissolution of Zn.
Keywords: ellipsometric perturbation analysis, aqueous corrosion, passivity, zinc hydroxide, zinc oxide, semiconductor thin film

---

1. Introduction

Zn is one of the most important metals in applications. Due to its oxidation propensity, Zn is a very efficient sacrificial anode in cathodic protection, and used as metallic coating [1]. For most applications, as well as in the deposition process of metallic coatings, electrochemical reactions on the Zn surface are of great importance. In recent years, ZnO as a semiconducting material with wide band gap of 3.4 eV has generated interest due its electronic properties [1–4]. ZnO is commonly found in the corrosion products of Zn and its alloys [1, 3]. The semiconducting properties of ZnO have been found to play an important role in the corrosion behaviour of Zn [1, 5–7]. Electrochemical works have shown that oxide films with different properties form in different electrolytes, some passivating the zinc surface better than others [1, 8].

A number of works focused on the electrochemistry of zinc over a range of pH values. The passivation of zinc, typically in alkaline media, has been investigated, and different kinds of passivating films have been proposed [1, 8–12]. Many passive films are amorphous or nanocrystalline [13, 14], with

broad distribution functions of distances and coordination numbers instead of sharp, well-defined values of crystals [3, 15, 16].

The complexity of the chemical – in addition to electrochemical – reactions on the Zn surface, in particular at alkaline pH, implies the need for additional surface characterisation, preferably in situ, as many of the potentially formed species are prone to structural changes during the drying process needed for modern surface analytics in UHV [1, 3, 16].

Ellipsometry in general is a sensitive optical method for the measurement of the optical constants and thicknesses of thin films [10, 17–19]. In situ ellipsometry can be performed during the modification process of a sample, which can be, e.g. the growth of a thin film, etching or cleaning of a sample [10, 20–23]. The technique enables the determination of fundamental process parameters, such as growth or etch rates and variation with time of optical properties, the latter related to structural changes. Surface reactions on many metals and metallic materials, such as iron, copper, steel, aluminium, zinc and sliver have been studied by this technique [2, 9, 21, 24, 25]. The thickness results obtained by ellipsometry, frequently as a result of fitting to an optical model, have been used to evaluate the growth mechanism and kinetics of oxide films on different metals [2, 9, 24, 25]. One result important for Zn is that after reduction for more than 10 min at a potential $E = -1.4$ V vs. saturated calomel electrode, a Zn surface without the presence of any oxide can be produced [9].

Ellipsometric measurements can either be performed at a single wavelength, or in a spectroscopic ellipsometry (SE) experiment at multiple wavelengths. In the latter case, the recording of spectral changes provides in-

formation on the interfacial electronic structure. SE can also be coupled to electrochemical experiments to study electrochemical reactions. The electrochemical activation and oxide growth on glassy carbon electrode was in situ measured by SE combined with other techniques [26]. The electrochemical oxidation of nickel and precipitation of hydroxide films was observed by in situ SE [27]. Recently, in situ SE has been used to monitor the transient growth and thinning of the passive film on Fe in borate buffer [20]. Moreover, the growth of oxide on a Zn substrate in different atmospheres has been investigated with in situ SE [28].

In this work, SE was used for in situ investigations of electrochemical processes on the Zn/electrolyte interface. Two different electrochemical experiments were performed to study the transformations on the surface, (a) cyclic voltammetry (CV) with dynamic potential scans and (b) chronoamperometry (CA) at certain static potentials, both in carbonate solution. Carbonate electrolyte was used as the complete exclusion of carbonate is difficult under ambient conditions, but affects the reactivity. An analysis based on the perturbation parameter of Lekner [29] is introduced and used to analyse the SE data.

2. Materials and Methods

2.1. Materials and sample preparation

Zn foil (99.95%, Goodfellow, Germany) with a thickness of 2 mm was cut into pieces of 20 mm × 30 mm. The sample was then mechanically ground with SiC paper up to 2500 grit, and subsequently further polished with final polishing suspension (100 nm SiO_2, pH = 9) to minimise surface roughness.

After that, these samples were sonicated in ethanol for 10 min and dried in a nitrogen stream. To reduce possible contamination and further oxidation, the sample after this treatment was directly put in the cell for electrochemical measurement. As the surface is already oxide-covered and was exposed to carbonate, surface reactions on the time-scale of the transfer are expected to have only a limited effect on the layer. The oxide is protecting the Zn, and after transfer is immersed in a solution similar to the previous one, so that the oxide/electrolyte interface is expected to be in a similar state as before the transfer. Therefore, no special transfer chamber to avoid contact with the outside air was constructed.

2.2. Design of optical-electrochemical cell

Details of the design of the sample cell were described in a different context elsewhere [28]. In addition to the previously described application of measurements in different gas atmospheres, the cell can also be filled and rinsed with different solutions. Four optical windows enable measurements at two incident angles, 50° and 70°. The cell contains a conventional three-electrode electrochemical setup. A platinum mesh as counter electrode and an Ag/AgCl/3M KCl electrode as reference electrode (DriRef-2SH microreference electrode, $E = +0.208$ mV vs. standard hydrogen electrode (SHE), World Precision Instruments Inc., USA) were used for electrochemical treatment. The connection of a metallic sample was realised by putting it in direct contact with the copper base part, which was connected to the working electrode connection of the potentiostat. In this work, all measurements were done at an incidence angle of 70°.

2.3. Electrochemistry

Electrochemical treatment of Zn was performed in 1.0 M Na_2CO_3 aqueous solution with a Gamry potentiostat (PHE200, Gamry Instruments Inc., USA) at room temperature (22 ± 2°C). Most data presented here were obtained in the cell described above. In this cell, the electrode surface area is well-defined, which is why the results of these measurements are presented as current densities I.

For reference, additional CV measurements were conducted in a standard electrochemical cell in a conventional three-electrode setup, where the current is flowing between the working electrode (i.e. the surface under study) and a counter electrode, while the reference electrode is used to precisely measure the electrode potential difference to the working electrode [30]. In this cell, the surface area A was difficult to determine because the electrode was Zn sheet with two sides and also the faces and corners exposed to the electrolyte. Therefore, for this cell (only in Fig. 1) current i instead of I is given.

2.4. Ellipsometry

In-situ SE measurements were performed using a UV-Vis spectroscopic ellipsometer (SE 800, Sentech Instruments GmbH, Germany) working in the wavelength range 297 nm – 820 nm (4.4 – 1.5 eV). In each measurement, data for 856 wavelengths were recorded on the instrument's CCD line detector. The light source was a Xenon lamp. For in situ measurements, the sample was mounted inside the optical-electrochemical cell described above.

In PCSA geometry [17], the polariser was fixed at an angle of +45°. Intensity measurements at 20 different analyser positions were used with and without a fixed retarder using the protocols implement in the instrument's

control software. For each wavelength λ in the range between 297 to 820 nm, the ellipsometric angles Ψ and Δ were extracted [31]. Ellipsometric spectra were acquired during CVs with a scan rate of 2 mV s^{-1} between +0.3 V and −1.7 V where acquisition of one spectrum took (43 ± 1) s, as well as during CA (−1.3, +0.2 and +1.2 V) measurements, where acquisition of one spectrum took (34 ± 1) s.

The angles Ψ and Δ were transformed into the ellipsometric ratio $\rho = \frac{r_p}{r_s} = \tan(\Psi)\exp(j\Delta)$ with $j = \sqrt{-1}$ [17]. This ratio of the amplitude reflection coefficients r_p and r_s for p- and s-polarised light, respectively, was analysed using a perturbation approach [29]. For individual layers and layer systems with a total thickness small compared to the wavelength, ρ is expanded to first order around a step profile in the dielectric function with ρ_0, yielding [29]

$$\rho = \rho_0 - \frac{2jq_1K^2(q_1+q_2)}{(q_1-q_2)\epsilon_1^2\epsilon_2(q_1/\epsilon_1+q_2/\epsilon_2)^2}J_1, \tag{1}$$

where the amplitude reflection coefficient $r_{s,0}$ of the step profile was replaced by the respective Fresnel equation [29]. Here,

$$K = \frac{2\pi\sqrt{\epsilon_1}}{\lambda}\sin(\theta_1) \tag{2}$$

is the wavevector component parallel to the interface at which a plane wave impinges under an angle of θ_1, while

$$q_o = \frac{2\pi\sqrt{\epsilon_o}}{\lambda}\cos(\theta_o), o \in 1,2 \tag{3}$$

is the wavevector component perpendicular to the interface in the respective medium, where index 1 indicates the medium of incidence and 2 indicates the Zn substrate. Literature values have been used for the wavelength-dependence of the dielectric function ϵ_1 of the electrolyte [32]. For the Zn

substrate, the Drude-Lorentz model with parameters previously reported has been used [7]. Eq. 1 can be solved for J_1 and used for a computation of J_1 from experimental data.

The perturbation parameter J_1 is related to the transition of the dielectric function of the interfacial region $\epsilon_l(z, \lambda)$ in z-direction (which is perpendicular to the interface) [29],

$$J_1(\lambda) = \int_{-\infty}^{\infty} \frac{[\epsilon_1(\lambda) - \epsilon_l(z, \lambda)]\,[\epsilon_l(z, \lambda) - \epsilon_2(\lambda)]}{\epsilon_l(z, \lambda)} \mathrm{d}z. \tag{4}$$

A measurement of the bare Zn/electrolyte interface without interfacial film may be difficult because of the reactivity of Zn [1, 33]. However, at cathodic potentials, complete removal of the surface oxide film has been reported [9], a result which is confirmed here. Therefore, ρ at cathodic potentials has been used as ρ_0. During CV, data for the potential range -1.4 V to -1.2 V has been averaged to obtain ρ_0. During CA, two measurements at -1.3 V have been averaged to calculate ρ_0.

2.5. Analysis of J_1

In the following, consider a homogeneous interfacial layer on top of the Zn substrate with an effective thickness d and an effective dielectric function $\epsilon_l(\lambda)$. For this case, eq. 4 simplifies to [29]

$$J_1(\lambda) = \frac{[\epsilon_1(\lambda) - \epsilon_l(\lambda)]\,[\epsilon_l(\lambda) - \epsilon_2(\lambda)]}{\epsilon_l(\lambda)} d. \tag{5}$$

Previously, the case of an absorbing layer on a non-absorbing substrate was treated in detail [29]. Further, for non-absorbing, anisotropic systems, first order [34, 35] and second order perturbation parameter [35] have been used to analyse interfacial properties of liquid crystals. Zinc oxide, hydroxide

and carbonate species to be investigated here do typically not absorb light at wavelengths in the upper part of the visible spectrum, therefore ϵ_l can be treated as purely real, i.e. $\epsilon_l = \mathrm{RE}(\epsilon_l)$ [7, 36]. Working on a metallic substrate, J_1 will nevertheless have an imaginary part. Therefore, here the case of a non-absorbing film on an absorbing substrate shall be considered.

The electrolyte is also non-absorbing, i.e. $\epsilon_1 = \mathrm{RE}(\epsilon_1)$. Further, the layer thickness is real, $d = \mathrm{RE}(d)$. Therefore, from eq. 5, two equations are obtained of real variables,

$$\mathrm{RE}(J_1) = \left[\epsilon_1 + \mathrm{RE}(\epsilon_2) - \epsilon_l - \frac{\epsilon_1}{\epsilon_l}\mathrm{RE}(\epsilon_2)\right] d \tag{6}$$

and

$$\mathrm{IM}(J_1) = \left(1 - \frac{\epsilon_1}{\epsilon_l}\right) \mathrm{IM}(\epsilon_2) d, \tag{7}$$

which can be solved for the two unknown quantities d and ϵ_l. (From the purely mathematical point of view, a similar approach can be used to invert ρ directly to d and ϵ_l in a ambient/layer/substrate system. However, a much higher precision in measurement is needed to yield stable results using such an approach compared to the perturbation approach.)

Taking the ratio of eq. 6 and 7 removes the dependence on d,

$$\frac{\mathrm{RE}(J_1)}{\mathrm{IM}(J_1)} = \frac{\epsilon_1 + \mathrm{RE}(\epsilon_2) - \epsilon_l - \frac{\epsilon_1}{\epsilon_l}\mathrm{RE}(\epsilon_2)}{(1 - \frac{\epsilon_1}{\epsilon_l})\mathrm{IM}(\epsilon_2)}. \tag{8}$$

Solving for ϵ_l yields

$$\epsilon_l = \mathrm{RE}(\epsilon_2) - \mathrm{IM}(\epsilon_2) \cdot \frac{\mathrm{RE}(J_1)}{\mathrm{IM}(J_1)}. \tag{9}$$

This result is subsequently substituted into eq. 6 or 7, which have then been solved for d. The structure of eq. 9 shows that this procedure is not applicable

for sample systems containing only non-absorbing materials, as in this case $\mathrm{Im}(J_1) = 0$.

While ϵ_l depends on the wavelength, d does not. One ellipsometric spectrum contains ρ at many wavelengths. Here, typically results for d obtained numerically from the procedure described for $\lambda > 650$ nm were averaged to yield d as reported in section 3. While for each value of d, 272 values at different wavelengths have been averaged, ϵ_l remains a function of the wavelength, so one point in the spectrum yields only a single ϵ_l. The data quality is not sufficient to analyse the spectral changes directly from J_1. Rather, information about the changes in the absorption spectrum are directly obtained from Ψ. Applying the analysis procedure described here to simulated data for a system Zn/ZnO/Air with different layer thicknesses of ZnO shows that the layer thickness obtained is typically 10-20 % too low, which is still considered as a physically reasonable result. Consequently, the obtained ϵ_l are too high, and sometimes take unphysically high values, which is a further reason for not discussing experimentally obtained values of ϵ_l.

The analysis here remains valid if a hydroxide layer instead of an oxide layer is present on the surface, and also if an hydroxide-terminated oxide layer is present. What limits the overall results is how close one can get experimentally to the "ideal" step profile in the refractive index. If, in the reference state, a hydroxidic termination is present on the surface, d can be interpreted as the increase in layer thickness with respect to the reference state. Effects of the ion distribution around the interface, though they can in principle be detected in ellipsometric experiments, are negligible due to the low refractive index contrast compared to the oxidic films.

3. Results and Discussion

3.1. Electrochemical behaviour of Zn in carbonate

Fig. 1 shows a typical CV of Zn in 1.0 M Na_2CO_3. Two anodic current peaks (A_1 and A_2), one anodic current plateau and two cathodic peaks (C_1 and C_2) were observed, consistent with [11]. According to [11], the oxidation current ($Zn \rightarrow Zn^{2+} + 2\ e^-$) on the bare metal is responsible for the oxidation peak A_1. A residual current passing through the already formed oxide/hydroxide film results in the current peak A_2, indicating that the oxide films formed in alkaline carbonate solution are rather porous. As Fig. 1 shows, the interfacial film is reduced at about -1.3 V. The reduction peaks C_1 and C_2 originate from a reduction current for ZnO and/or $Zn(OH)_2$ and the redeposition current for Zn^{2+}, respectively. At lower potentials, active surface was present and H_2 evolution is observed.

3.2. In situ SE during CV

Ellipsometric measurements have been performed to determine the change of the interfacial structure during reduction and subsequent oxidation. During a dynamic potential scan as in a CV measurement, the potential range over which a single SE spectrum averages depends on the scan rate. If the same scan rate as in Fig. 1 were applied during in situ SE measurements, the potential range for each SE spectrum will be too wide (50 mV/s $\cdot$ 43 s = 2.15 V) and the results can not be used to probe potential-dependent surface features. Thus, a scan rate of 2 mV/s was used. At 2 mV/s, each SE spectrum averages over $\approx$85 mV.

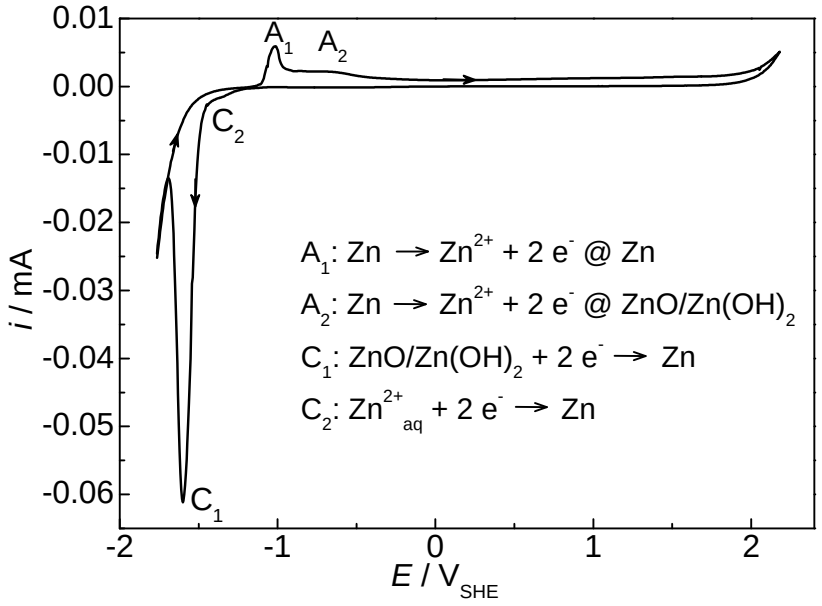

Figure 1: CV of polycrystalline Zn in 1.0 M Na_2CO_3 in electrochemical cell. Scan rate: 50 mV/s. Peak assignments according to [11].

Fig. 2 shows the CV at a scan rate of 2 mV/s and the thickness d of the interface film (calculated following the procedure outlined in section 2.5) as function of potential during a CV scan. Before cycling the potential, one SE measurement was performed at open circuit potential (OCP), i.e. at the potential which spontaneously forms when putting into contact an electrode and an electrolyte (empty square in Fig. 2). The OCP itself has not been measured, and the point has been arbitrarily placed on the potential axis. Subsequently, E was changed to the the positive limit, +0.3 V, and a CV measurement was started. At this potential, Zn is covered with an oxidic layer. The film thickness at open circuit potential (OCP) is about 0.8 nm. With the application of an anodic potential, the thickness jumps to a value of ≈2.2 nm on a time scale below the experimental resolution. During scanning in cathodic direction, a gradual decrease of the thickness was observed till −0.96 V. Upon further reduction, the thickness decreases at a rate of ≈ 8 nm/V, it reaches almost zero at a potential of −1.13 V and keeps constant till −1.48 V. In this potential range, as displayed in the CV in Fig. 2, two cathodic peaks are observed. The cathodic peaks indicate the reduction of oxidised species, resulting in a substantial thinning of the oxide film. All of these features can be directly observed by in situ SE. In the CV, one more broad reduction peak (−1.20 V to −1.45 V) was observed after the first reduction peak (−1.13 V) which does coincide with a region of constant thickness of the interfacial layer. This behaviour was attributed to the fact that the first cathodic peak is due to the reduction of previously formed oxide/hydroxide, while the second reduction peak was due to the redeposition of Zn from previously dissolved Zn^{2+} ions present in the

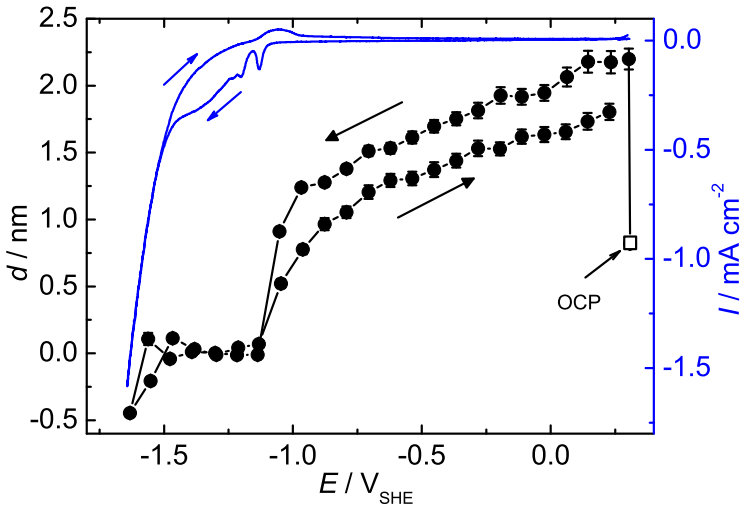

Figure 2: Calculated thickness (■, scale on the left) during a CV (line, scale on the right) at a scan rate of 2 mV/s. The open square (□) is an initial measurement at OCP without electrodes connected.

solution in this case. Thus, a cathodic current peak was observed without the further change of oxide layer thickness between −1.20 V to −1.45 V. This result confirms previous conclusions from purely electrochemical work about the current peaks in the CV [11, 12]. From −1.48 to −1.70 V, there are jumps in the value of the thickness, attributed to the starting H_2 evolution reaction and the consequent presence of adsorbed H_2, which leads to formation of macroscopic bubbles. At the same time, a fast increase of the cathodic current is observed in CV (Fig. 2).

After reversal of the scan direction, no obvious change is seen for the thickness till the potential reaches −1.13 V, where the oxidation peak A_1 starts. Upon further positive scanning, the thickness increases with ≈5 nm/V

between -1.13 V and -0.96 V (where peak A_1 ends). At higher potentials, a drop in current to a plateau value is observed. During this plateau, the thickness increases almost linearly with potential at 1.0 nm/V. Such a linear growth with increasing potential was found for surface layers on metals in the passive region of the current-potential diagram [20], though other behaviour was reported for Zn in borate buffer [2]. Linear increase of layer thickness in the passive regime is consistent with what is called the "point defect model" of passive films [37, 38]. From the electrochemical point of view, the oxide film formed here is not too "passive", as the residual current density is $3-10$ μA cm^{-2}.

The anodic current measured during the CV can be used to evaluate the net integral amount n_{Zn} of Zn over time t which is oxidised to Zn^{2+}, assuming that only Zn oxidation following the reaction $Zn \rightarrow Zn^{2+} + 2\ e^-$ contributes to the current i as

$$n_{\mathrm{Zn}}(E) = \frac{1}{2eN_A} \int_{E(i=0)}^{E} i(t)\mathrm{d}t, \tag{10}$$

with Avogadro's constant N_A and the elementary charge e. The resulting dependence of n_{Zn} on potential is shown in Fig. 3a. The oxidised Zn^{2+} is expected to be distributed mainly to three different species: dissolved Zn^{2+}_{aq}, $Zn(OH)_2$ and ZnO. Detailed ex situ analysis of the resulting layers, which is not topic of this work, shows that only traces of carbonate are present on the surface, which is why carbonate species are not considered for the analysis.

From n_{Zn} and d, an effective concentration c_{Zn} of Zn^{2+} in the layer is obtained (A - electrode surface area),

$$c_{\mathrm{Zn}} = \frac{n_{\mathrm{Zn}}}{Ad}. \tag{11}$$

The potential/time dependence of d was obtained by linear interpolation

between the points at which measurements were performed. Fig. 3b shows c_{Zn} divided by $c_{\mathrm{ZnO}} = 1/V_M(\mathrm{ZnO})$, the reciprocal molar volume V_M of crystalline ZnO, $c_{\mathrm{ZnO}} = 6.9 \cdot 10^4$ mol/m^3 [32]. The ratio $c_{\mathrm{Zn(OH)_2}}/c_{\mathrm{ZnO}}$ with $c_{\mathrm{Zn(OH)_2}} = 3.1 \cdot 10^4$ mol/m^3 [32] is shown for reference as a line. Different values of $c_{\mathrm{Zn}}/c_{\mathrm{ZnO}}$ can be understood considering $c_{\mathrm{Zn}}/c_{\mathrm{ZnO}} \propto Q/d$ with the net transferred charge Q. If only metal dissolution without formation of a layer is going on, $d \to 0$, hence $c_{\mathrm{Zn}}/c_{\mathrm{ZnO}} \to \infty$. If a layer of crystalline ZnO is formed, $c_{\mathrm{Zn}}/c_{\mathrm{ZnO}} = 1$. For amorphous ZnO films, values slightly lower than 1 are expected. If the product of oxidation is $Zn(OH)_2$, $c_{\mathrm{Zn}}/c_{\mathrm{ZnO}} = c_{\mathrm{Zn(OH)_2}}/c_{\mathrm{ZnO}} \approx 0.45$. Cases with strongly swollen networks result in $c_{\mathrm{Zn}}/c_{\mathrm{ZnO}} < c_{\mathrm{Zn(OH)_2}}/c_{\mathrm{ZnO}}$. In addition, $c_{\mathrm{Zn}}/c_{\mathrm{ZnO}} << 1$ is also expected if the layer grows by precipitation from solution rather than electrochemically.

The graph in Fig. 3b rises sharply from zero to ≈3.3. The sharp increase, which goes already beyond the value of 1.0 required for direct ZnO formation, shows that initially, the current increase results in metal dissolution. In the region of linear thickness growth, $c_{\mathrm{Zn}}/c_{\mathrm{ZnO}}$ rises only marginally from 3.3 to 4.0. The current flowing in this potential regime therefore mainly results in a thickening of the interfacial film, and only to a lower extend in metal dissolution. More information of the nature of the surface film can be obtained by analysing the spectra.

Fig. 4 shows the real and imaginary part of J_1 as a function of potential for different wavelengths during the CV scan. For all wavelengths, $\mathrm{Re}(J_1)$ behaves the same as that of the calculated oxide thickness which was extracted from high wavelength data only. This fact shows that the assumption of small changes in the refractive index in the oxide layer is justified. The behaviour

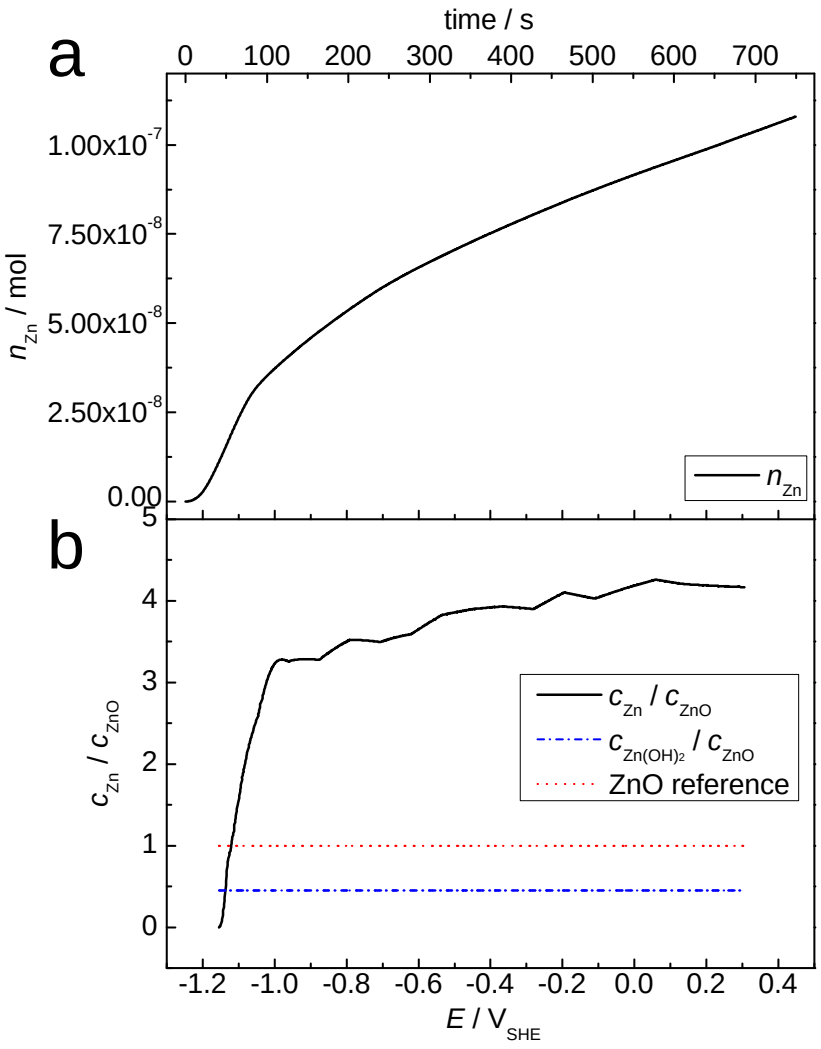

Figure 3: (a) The amount n_{Zn} of Zn which is oxidised to Zn^{2+}; (b) $c_{\mathrm{Zn}}/c_{\mathrm{ZnO}}$ during the reversed positive scan between -1.15 V and 0.3 V in the CV shown in Fig. 2. The dash-dot line in (b) shows $c_{\mathrm{Zn(OH)_2}}/c_{\mathrm{ZnO}}$.

of $\mathrm{Im}(J_1)$ is different. At wavelength of 700 nm and 650 nm, $\mathrm{Im}(J_1)$ has the same magnitude as as $\mathrm{Re}(J_1)$. The agreement between imaginary and real part in this wavelength region confirms the assumption that the imaginary part in this region of the spectrum is governed by the substrate and the films are non-absorbing. For lower wavelengths, absorption in the thin oxide films leads to differences, e.g. at 350 nm, at a photon energy above the ZnO bandgap, $\mathrm{Im}(J_1)$ is close to zero. Therefore, these wavelengths have not been used in the analysis of the thickness, but they can be used to analyse changes in the electronic structure of the oxide films.

Changes in the electronic structure are directly manifested in the ellipsometric parameter Ψ. Fig. 5 shows the lower wavelength region of spectra of Ψ during the CV. The bending at $\approx$380 nm is a typical feature for the formation of zinc oxide, as it is related to the main electronic absorption of ZnO, which, because of the surface selection rule, affects the amplitude reflection coefficient in p-polarisation, but not in s-polarisation, hence leading to an absorption feature in the spectrum [28]. No film absorption is visible for the initially mechanically polished Zn substrate [7]. The first curve (front black) is Ψ prior to the application of an electrochemical potential. The bending at 380 nm is not observed. After switching E to +0.3 V the measured Ψ changes immediately, the typical bend at 380 nm is observed (second curve in Fig. 5), and remains present while scanning in cathodic direction. During negative scanning, the feature becomes more pronounced and disappears at strongly cathodic potentials. The apparent contradiction that the absorption feature increases while the layer thickness decreases can be understood as the superposition of a potential-dependent phenomenon,

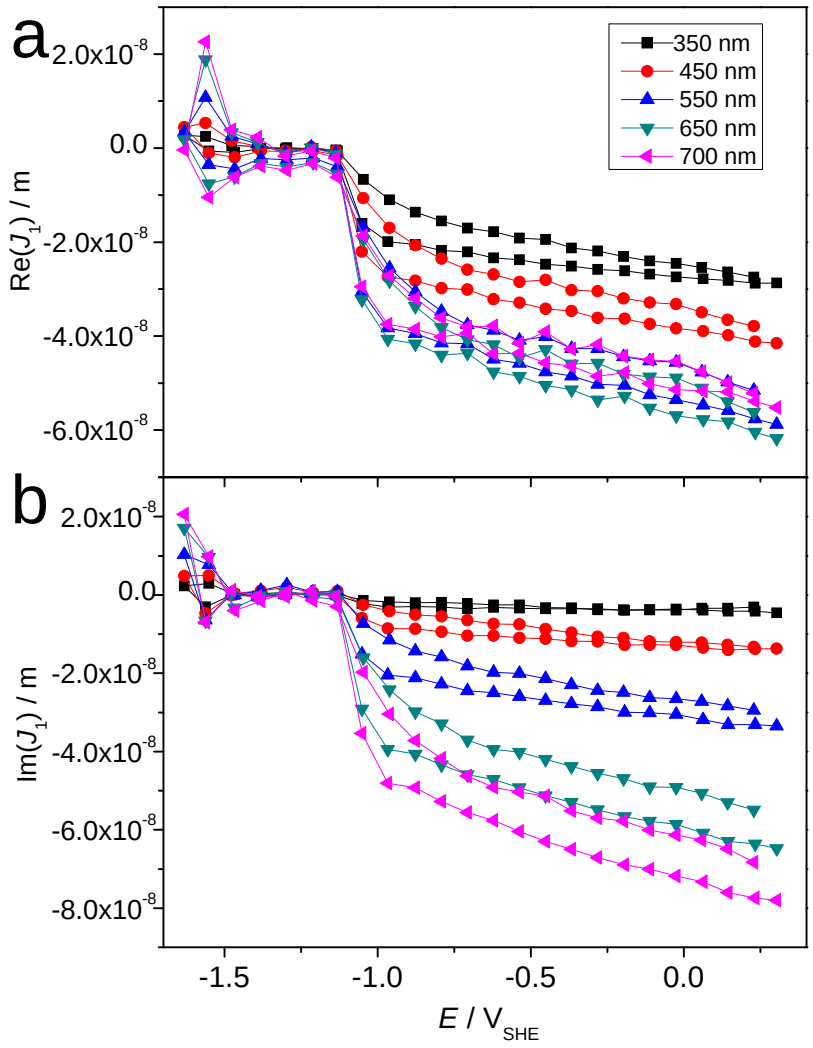

Figure 4: Real (a) and imaginary (b) part of J_1 at different wavelengths as indicated in the graph for different potentials during the CV shown in Fig. 2.

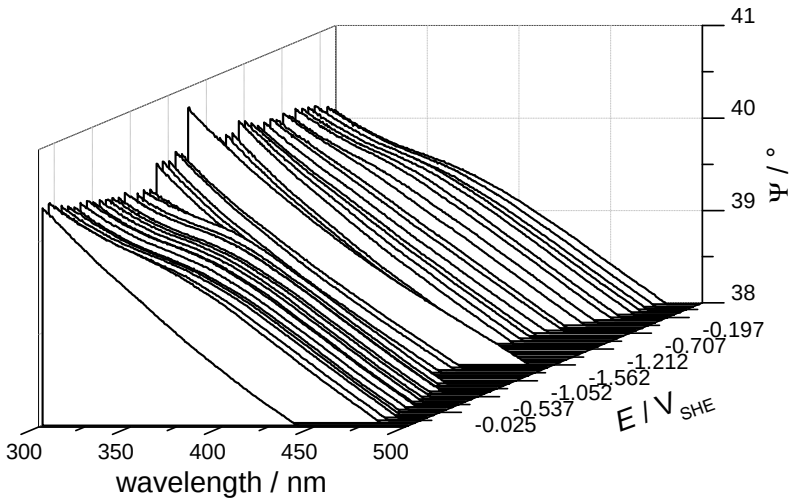

Figure 5: Spectra of Ψ for different potentials during the CV.

i.e. the reduction of oxide from the ZnO layer, with a time-dependent phenomenon, the ageing of the oxidic film. As shown in Fig. 2, d jumps from 0.8 nm to 2.2 nm on the application of an anodic potential, with a subsequent gradual decrease during negative scanning. In the potential window of the cathodic reduction peak C_2, the thickness decreased from more than 2 nm to almost zero, indicating the disappearance of oxide. In the same potential window, the absorption <380 nm in Ψ also disappeared. During the reversed positive scanning, the bend in Ψ at 380 nm was not observed until the potential reached -0.6 V, subsequently becoming more pronounced with further potential increase. The absence of the absorption feature in the spectra of Ψ at potentials below -1.1 V is a good indicator that oxide is indeed absent in this potential regime, which confirms previous works [9].

The fact that there is only a small increase of c_{Zn} during the phase of linear

thickness growth, and at the same time the ZnO absorption in the spectrum becomes more pronounced while in the reductive scan also an increasing prominence of the oxidic absorption is observed leads to the following model. Upon oxidation, $Zn(OH)_2$ is initially formed on the surface. This hydroxide ages transforming into ZnO, while the layer thickness remains constant during this process. Newly formed species will always be hydroxide, which ages at a certain rate, keeping the overall density constant with increasing thickness.

3.3. In situ SE and CA during potentiostatic oxide growth

In the CV experiments, the separation of time-dependent and potential-dependent features is not always possible. To have a more precise control, the growth kinetics of the interfacial film on Zn during a potentiostatic process was investigated. Fig. 6 shows the applied potential (a) and the corresponding current (b) from a CA experiment. The sample was first reduced at -1.3 V for 60 min, then anodically oxidised initially at $+0.2$ V and subsequently at $+1.2$ V for 60 min each. At the potential of -1.3 V (Fig. 1 and 2), the oxide present on the surface of Zn is reduced. During the cathodic reduction and further anodic oxidation processes, in situ SE was measured to determine the behaviour of the oxide film. Fig. 6c indicates the thickness calculated through the perturbation approach (section 2.5). Upon application of the cathodic potential (Fig. 6b) the cathodic current diminishes fast, and after 30 s, the current reaches constant value close to 0, remaining constant throughout this potential stage.

The thickness of the film (Fig. 6c) follows closely the applied potential. Because of the low speed of each SE measurement (>30 s) and the fast re-

duction process, the first measurement was complete after the fast reduction process finished. The film thickness during the complete reduction period was close to zero. The noise in the thickness data between 15 and 30 min measurement time is tentatively attributed to entrapment of a gas bubble in the optical path.

Zn is oxidised at potentials above -0.5 V. Fig. 6b shows the current response after the applied potential is changed from -1.3 V to $+0.2$ V and subsequently from $+0.2$ to $+1.2$ V. The current density changes to an anodic maximum of $\approx$160 μA/cm^{-2} in $<$1 s. Subsequently, the current decreases within $\approx$1 min to less than 15 μA cm^{-2}. At the same time, the thickness of the oxide film increases from almost zero to $\approx$ 1.9 nm. The increased noise in the thickness results around the first potential jump originate from the fact that the resulting values of J_1 are in a region of extremely high sensitivity to layer parameters. Here, the data analysis procedure does hardly provide stable results, which is reflected in extremely large errors of these values, which are not shown as they would dominate the plot. In regions with stable results (times before 60 min and after 75 min), the statistical uncertainty of the thickness is $\approx$0.2 nm. After the fast initial current decrease, the current decreases slowly with time, as shown in detail in the inset in Fig. 6b. The anodic current originates from the oxidation process of Zn on the surface, and the non-zero value of the current indicates a slow but continuous growth of oxide on the electrode surface. In the region where the analysis procedure yields stable results, the thickness for higher times indeed shows a slow increase with time. A closer look into the current response (Fig. 6b inset) also indicates a current decrease after $\approx$30 min. Afterwards, $I \approx 2-3$

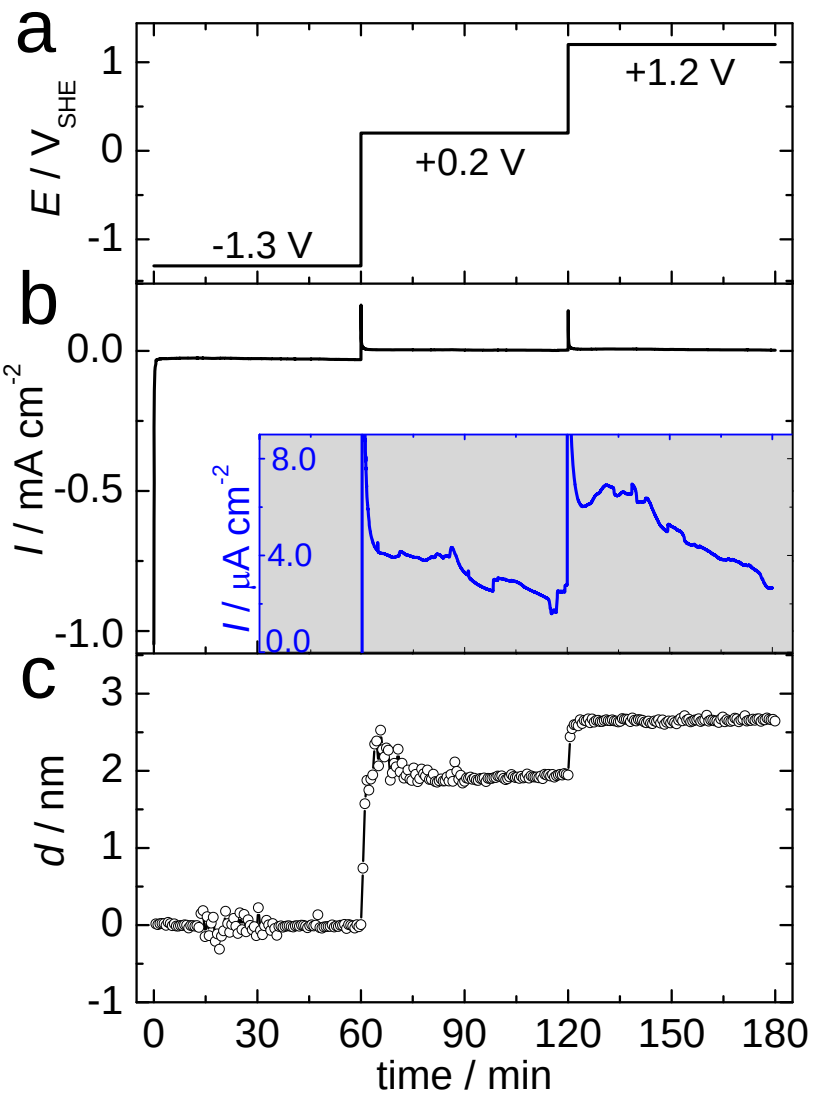

Figure 6: (a) Applied potential profile, 0−60 min: −1.3 V, 60−120 min: +0.2 V, 120−180 min: +1.2 V; (b) corresponding current densities (inset: enlarged plot of current density from 60 min to 120 min) and (c) thickness as a function of time. Errors of the thickness are ≈0.2 nm

μA cm^{-2}.

A further increase in the thickness of the oxide film is observed when the potential is increased from +0.2 V to +1.2 V. As observed during the first jump, the layer thickness increases is fast during the potential jump to 2.4 nm, and a further slow growth leads after 1 h to a value of 2.7 nm.

An integration of the current as explained in Sec. 3.2 (eq. 10) and determination of c_{Zn} (11) was performed for the CA data. The results are displayed in Fig. 7. Comparing the increase in n_{Zn} to the increase in thickness (Fig. 6c) shows major differences in the time-evolution of the curves. The initial current spike contains only a relatively small ($\approx$10 %) fraction of the totally transferred charge, but almost the complete growth in thickness. (In the analysis here, the possibility of having missed a relatively large portion of the current due to the limited bandwidth of the potentiostat is disregarded.) The ratio $c_{\mathrm{Zn}}/c_{\mathrm{ZnO}}$ reaches 0.5 within the first 30 s after the potential jump, and increases above 1 after 5 min. These results indicate that metal dissolution into the electrolyte is occurring at these potentials through the oxide layer, which does not grow in size. During the second potential jump, the ratio $c_{\mathrm{Zn}}/c_{\mathrm{ZnO}}$ decreases initially, although n_{Zn} increases. This result can be easily explained by the formation of another layer on the surface of the first layer. This layer experiences a subsequent densification.

Fig. 8 shows the plot of real and imaginary part of J_1 at different applied potentials for different wavelengths. The time evolution of these curves leads to the same conclusions as drawn for the CV measurements, namely that absorption of the film changes during the potential treatment.

Fig. 9a shows the data for Ψ from the SE measurements during CA. The

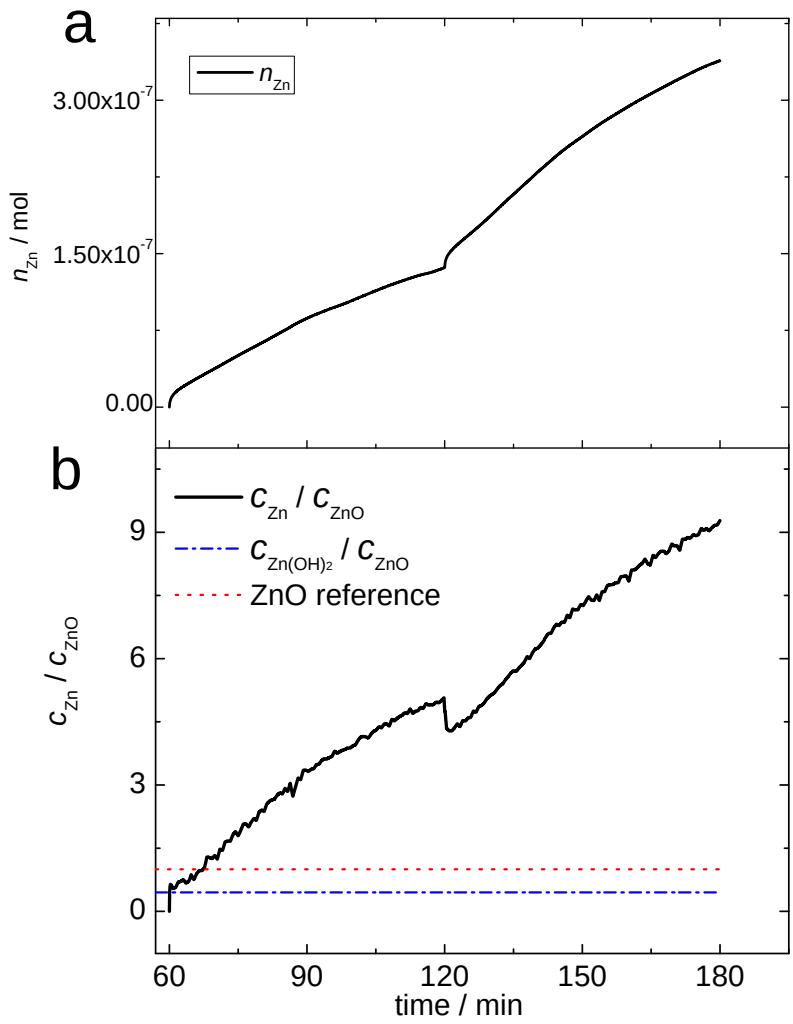

Figure 7: (a) Amount n_{Zn} of Zn which is oxidised to Zn^{2+}; and (b) the ratio between c_{Zn} and c_{ZnO} during CA. The dash-dot line in (b) shows $c_{\mathrm{Zn(OH)_2}}/c_{\mathrm{ZnO}}$.

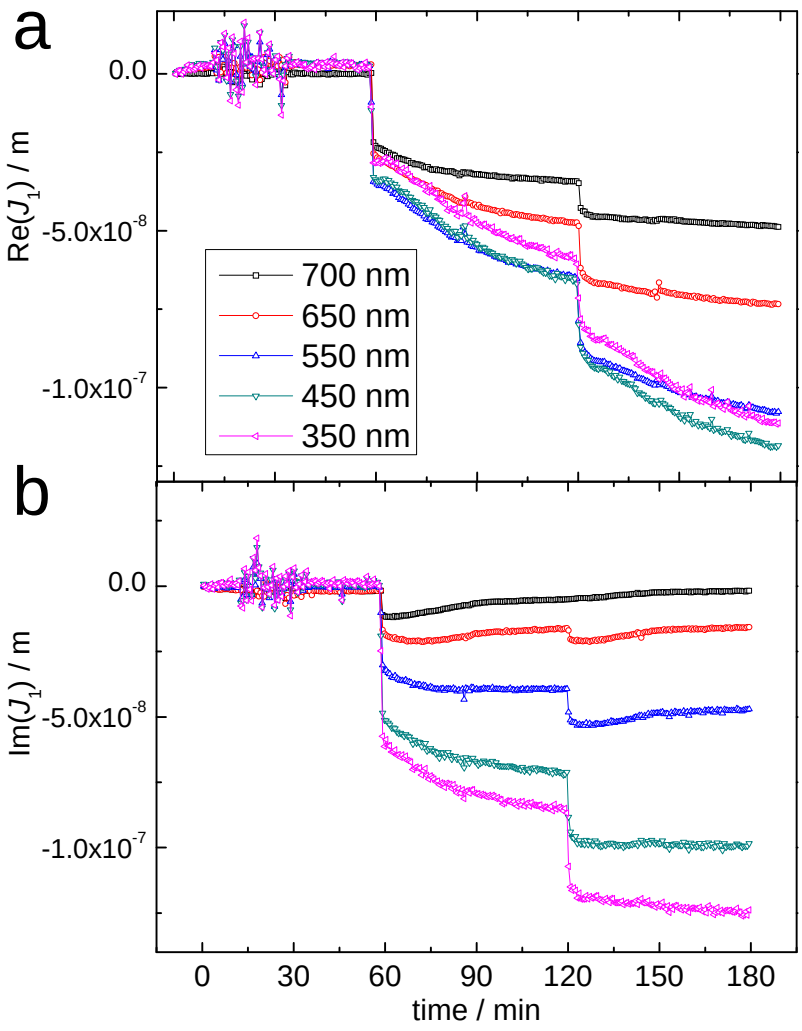

Figure 8: Real (a) and imaginary (b) part of J_1 at different wavelengths as indicated in the graph during the CA measurements shown in Fig. 6.

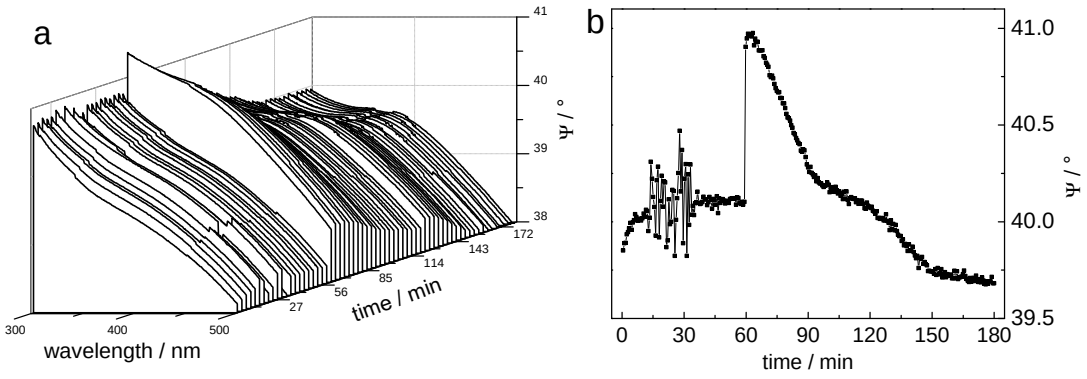

Figure 9: (a) Plot of the measured Ψ with time during the chronoamerometry. (b) Ψ at wavelength of 350 nm during the chronoamerometry

bending of Ψ at 380 nm is absent at a potential of -1.3 V. After switching the potential from -1.3 to $+0.2$ V, Ψ changes immediately, and the bending of Ψ at 380 nm, which indicates the presence of an absorption, becomes more and more pronounced. Fig. 9b shows the evolution with time of Ψ at 350 nm as an example of the overall curve, which also shows changes within 30 min after the respective potential jump. This behaviour indicates the continuous transformation of the layer into a "mature" oxide layer with only a small increase in thickness of the layer. After both potential jumps, this change in the absorption spectrum of the layer stops after 30 min, after which curve enters a second phase. The same second phase is also observed in the integrated currents in Fig. 7, which continues to increase with a slightly lower slope. The behaviour indicates that an initially formed layer is transforming gradually into a layer of ZnO. In the second phase, metal dissolution is still occurring, at a constant absorption spectrum (and hence, electronic structure) of the oxide layer.

4. Summary and Conclusions

During both potentiostatic treatment of zinc as well as CV measurements in alkaline carbonate solution, an analysis of ellipsometric data on the basis of Lekner's perturbation parameter enables a direct determination of the layer thickness of the interfacial region without the need of an optical model. Additionally, the analysis of the ellipsometric parameter Ψ yields insight into the change in the absorption spectra of the interfacial region.

During dynamic potential scanning, the thinning of the oxide during the negative scanning and subsequent growth of oxide in the reversed positive scanning on Zn can be followed. CV-like plots in the format of thickness, real or imaginary part of the perturbation parameter instead of current as the function of potential are obtained. The thickness of the interfacial film, which consists mainly of ZnO, grows linearly with potential at potentials above the potential of the A_2 current peak. This behaviour is found for passive materials as well. The characteristic electronic absorption of ZnO is present in the films in this potential regime.

Results of potential jump experiments show that the interfacial oxide layer grows in thickness rapidly upon the application of anodic potentials within the time scale of less than 1 min, and the increasing of the thickness during the subsequent 59 min is lower than that during the first minute. The electronic absorption of ZnO occurs quickly and subsequently takes a certain time ($\approx$30 min) to fully evolve in the spectra, showing an ageing of the interfacial layer. The analysis of the concentration of Zn^{2+} in the layer indicates an ongoing dissolution of Zn into the electrolyte. The rate of Zn dissolution needs to be measured independently by analysis of the electrolyte

to verify that the residual current is related mainly to metal dissolution.

More information about the electronic structure of the interfacial films are expected to be obtained form a more detailed analysis of $\epsilon_l(\lambda)$. It is especially promising to analyse the changes in the spectra of a dynamic system, i.e. while Zn transport during the layer is ongoing, as is the case here in during the CA measurements. The ageing observed here may be related to the ongoing transport of zinc through the layer. A comparison to passive materials with very low residual currents of dissolution should allow conclusions about this behaviour. With increased time resolution of the ellipsometric experiments, more details about the initial stages of the layer formation will be obtained.

5. Acknowledgement

Y. C. thanks for support from the European Union and the state of North Rhine-Westphalia in the frame of the HighTech.NRW program. The authors thank P. Schneider for his help in the design of the optical-electrochemical cell. Prof. Stratmann is acknowledged for his continuous support.

References

[1] X. Zhang, Corrosion and Electrochemistry of Zinc, Plenum Press, New York, 1996.

[2] J. Buchholz, Surf. Sci. 101 (1980) 146–154.

[3] J. W. Schultze, A. W. Hassel, in: Encyclopedia of Electrochemistry, volume 4, Wiley-VCH, pp. 216–235.

[4] H. von Wenckstern, H. Schmidt, M. Brandt, A. Lajn, R. Pickenhain, M. Lorenz, M. Grundmann, D. Hofmann, A. Polity, B. Meyer, H. Saal, M. Binnewies, A. Borger, K.-D. Becker, V. Tikhomirov, K. Jug, Prog. Solid State Chem. 37 (2009) 153–172.

[5] P. Lang, C. Nogues, Surf. Sci. 602 (2008) 2137–2147.

[6] G. Ballerini, K. Ogle, M. G. Barthes-Labrousse, Appl. Surf. Sci. 253 (2007) 6860–6867.

[7] J. Zuo, A. Erbe, Phys. Chem. Chem. Phys. 12 (2010) 11467–11476.

[8] M. Mokaddem, P. Volovitch, K. Ogle, Electrochim. Acta 55 (2010) 7867 – 7875.

[9] A. Hamnett, R. J. Mortimer, J. Electroanal. Chem. 234 (1987) 185–192.

[10] A. Hamnett, J. Chem. Soc. Faraday Trans. 89 (1993) 1593–1607.

[11] D. C. W. Kannangara, B. E. Conway, J. Electrochem. Soc. 134 (1987) 894–906.

[12] B. E. Conway, D. C. W. Kannangara, J. Electrochem. Soc. 134 (1987) 906–918.

[13] J. L. Delplancke, R. Winand, Electrochim. Acta 33 (1988) 1539–1549.

[14] J. L. Delplancke, R. Winand, Electrochim. Acta 33 (1988) 1551–1559.

[15] J. W. Schultze, L. Elfenthal, K. Leitner, O. Meyer, Electrochim. Acta 33 (1988) 911–925.

[16] X.-L. Shang, B. Zhang, E.-H. Han, W. Ke, Electrochim. Acta 56 (2011) 1417–1425.

[17] R. M. A. Azzam, N. M. Bashara, Ellipsometry and Polarized Light, Elsevier Science, Amsterdam, 1999.

[18] H. Fujiwara, Spectroscopic Ellipsometry: Principles and Applications, John Wiley & Sons, Chichester, 2007.

[19] H. G. Tompkins, E. A. Irene (Eds.), Handbook of Ellipsometry, Willam Andrew Publishing - Springer Verlag, Norwich, Heidelberg, 2005.

[20] Z. Lu, D. D. Macdonald, Electrochim. Acta 53 (2008) 7696–7702.

[21] J. D. Sloppy, N. J. Podraza, E. C. Dickey, D. D. Macdonald, Electrochim. Acta 55 (2010) 8751 – 8757.

[22] N. Hara, Y. Kobayashi, D. Kagaya, N. Akao, Corr. Sci. 49 (2007) 166 – 175.

[23] S. Joo, I. Muto, N. Hara, J. Electrochem. Soc. 155 (2008) C154–C161.

[24] P. Hayfield, Surf. Sci. 56 (1976) 488–507.

[25] M. Lopez Teijelo, J. O. Zerbino, J. R. Vilche, A. J. Arvia, Electrochim. Acta 29 (1984) 939–946.

[26] M. G. Sullivan, B. Schnyder, M. Bartsch, D. Alliata, C. Barbero, R. Imhof, R. Kotz, J. Electrochem. Soc. 147 (2000).

[27] F. P. Kong, R. Kostecki, F. McLarnon, R. H. Muller, Thin Solid Films 313 (1998) 775–780.

[28] Y. Chen, P. Schneider, A. Erbe, Phys. Stat. Sol. A (2012) , DOI: 10.1002/pssa.201100542.

[29] J. Lekner, Theory of Reflection of Electromagnetic and Particle Waves, M. Nijhoff, Dordrecht, 1987.

[30] C. M. A. Brett, A. Brett, Electrochemistry - Principles, Methods, and Applications, Oxford University Press, Oxford, 1994.

[31] U. Richter, Thin Solid Films 313-314 (1998) 102–107.

[32] D. R. Lide (Ed.), Handbook of Chemistry and Physics, CRC Press, Boca Raton, 90th edition, 2009.

[33] M. Pourbaix, Atlas of Electrochemical Equilibria in Aqueous Solutions, National Association of Corrosion Engineers, Houston, 2nd edition, 1974.

[34] R. Sigel, G. Strobl, J. Chem. Phys. 112 (2000) 1029–1039.

[35] H. Kasten, G. Strobl, J. Chem. Phys. 103 (1995) 6768–6774.

[36] P. Washington, H. Ong, J. Dai, R. Chang, Appl. Phys. Lett. 72 (1998) 3261–3263.

[37] D. D. Macdonald, J. Electrochem. Soc. 139 (1992) 3434–3449.

[38] G. S. Frankel, N. Sridhar, Mater. Today 11 (2008) 38–44.

Highlights

- thickness determination from ellipsometry without optical model
- ZnO thickness increases linearly with potential in the "pseudo-passive" regime
- density of interfacial layer in constant during potential increase
- potentiostatic treatment shows an aging of the interfacial layer to yield ZnO
- absorption spectrum of the oxide is modified by metal transport

Graphical abstract